Articles

NMR Solution Structure of the Antitumor Compound PT523 and NADPH in the Ternary Complex with Human Dihydrofolate Reductase†

Jason M. Johnson,‡ Elizabeth M. Meiering,§,|| Joel E. Wright,⊥ Jorge Pardo,⊥ Andre Rosowsky,⊥ and Gerhard Wagner*,§

Program for Higher Degrees in Biophysics, Department of Biological Chemistry and Molecular Pharmacology, Harvard Medical School, 240 Longwood Avenue, and Dana-Farber Cancer Institute, 44 Binney Street, Boston, Massachusetts 02115

Received December 11, 1996; Revised Manuscript Received January 31, 1997⊗

ABSTRACT: The antitumor compound PT523 [N^{α}-(4-amino-4-deoxypteroyl)-N^{δ}-hemiphthaloyl-L-ornithine] was found to have an inhibition constant (K_i) of 0.35 ± 0.10 pM against human dihydrofolate reductase (hDHFR), 15-fold lower than that of the classical antifolate drug methotrexate (MTX). The structure of PT523 bound to hDHFR and hDHFR−NADPH was investigated using multinuclear NMR techniques. NMR data indicate that the binary complex has two distinct conformations in solution which are in slow exchange and that the addition of NADPH stabilizes the ternary complex in a single bound state. Comparison of resonance assignments in the PT523 and MTX ternary complexes revealed that substantial protein chemical shift differences are limited to small regions of hDHFR tertiary structure. A restrained molecular dynamics and energy minimization protocol was performed for the hDHFR−PT523−NADPH complex, using 185 NOE restraints (33 intermolecular) to define the ligand-binding region. The positions of the pteridine and pABA rings of PT523 and the nicotinamide and ribose rings of NADPH are well defined in the solution structures (RMSD = 0.59 Å) and are consistent with previously determined structures of DHFR complexes. The N^{δ}-hemiphthaloyl-L-ornithine group of PT523 is less well defined, and the calculated model structures suggest the hemiphthaloyl ring may adopt more than one conformation in solution. Contacts between the hemiphthaloyl ring and hDHFR, which are not possible in the hDHFR−MTX−NADPH complex, may explain the greater inhibition potency of PT523.

Human dihydrofolate reductase, a 186-residue (21.5 kDa), monomeric protein, catalyzes the reduction of 7,8-dihydrofolate (FH_2, **1**) to 5,6,7,8-tetrahydrofolate (FH_4) using NADPH (**5**) as a cofactor (see Chart 1). FH_4 and its derivatives are necessary for the biosynthesis of thymidylate, purine nucleotides, and several amino acids. There is considerable pharmacological interest in DHFR,[1] because inhibitors of the enzyme such as methotrexate (MTX, **2**) decrease intracellular FH_4 levels and can thus cause aberrant DNA synthesis and cell death in proliferating cells. MTX and other antifolate drugs are commonly used in cancer chemotherapy and in antimicrobial and immunosuppressive treatments.

In order to understand the specificity of ligand binding, and to be able to design new drugs with predictable binding properties, structural comparisons of closely related protein−ligand complexes are necessary. Complexes of DHFR with many different ligands have been studied, particularly for DHFRs from *Escherichia coli*, *Lactobacillus casei*, and chicken liver, making the enzyme one of the best available model systems for understanding binding specificity and structure−function relationships [for reviews, see Blakley (1984, 1995), Freisheim and Matthews (1984), and Kraut and Matthews (1987)]. The structures of DHFR complexes from several species have been determined by X-ray crystallography [for references, see Kraut and Matthews (1987), McTigue *et al.* (1992), and Blakley (1995)], including human enzyme in the binary complex with folate and 5-deazafolate (Oefner *et al.*, 1988; Davies *et al.*, 1990) and in the ternary

† J.M.J. was supported by a grant from the National Science Foundation, J.E.W. and A.R. were supported by Grant RO1-CA25394 from the National Cancer Institute, and E.M.M. was supported by a fellowship from the Jane Coffin Childs Fund for Medical Research.

* Author to whom correspondence should be addressed.

‡ Program for Higher Degrees in Biophysics, Harvard University, Harvard Medical School, 240 Longwood Ave., Boston, MA 02115.

§ Department of Biological Chemistry and Molecular Pharmacology, Harvard Medical School.

|| Present address: Department of Chemistry, University of Waterloo, Waterloo, Ontario N2L 3G1, Canada.

⊥ Dana-Farber Cancer Institute and Department of Biological Chemistry and Molecular Pharmacology, Harvard Medical School.

⊗ Abstract published in *Advance ACS Abstracts,* March 15, 1997.

[1] Abbreviations: 1D, one dimensional; 2D, two dimensional; 3D, three dimensional; DHFR, dihydrofolate reductase (EC 1.5.1.3); hDHFR, human DHFR; DQF-COSY, double-quantum-filtered correlation spectroscopy; FH_2, 7,8-dihydrofolate; FH_4, 5,6,7,8-tetrahydrofolate; HMQC, heteronuclear multiple-quantum coherence spectroscopy; HNHA, ^{15}N-separated quantitative *J*-correlation spectroscopy; HSQC, heteronuclear single-quantum coherence spectroscopy; MTX, methotrexate (8-amino-10-methylpteroylglutamic acid); MTXγT, methotrexate-γ-tetrazole; NADPH, reduced nicotinamide adenine dinucleotide phosphate; NIST, National Institute of Standards and Technology; NOE, nuclear Overhauser effect; NOESY, two-dimensional nuclear Overhauser effect spectroscopy; pABA, *p*-aminobenzoic acid; PAGE, polyacrylamide gel electrophoresis; PT523, N^{α}-(4-amino-4-deoxypteroyl)-N^{δ}-hemiphthaloyl-L-ornithine; RMSD, root mean square deviation; ROESY, rotating frame NOE spectroscopy; TOCSY, total correlation spectroscopy.

S0006-2960(96)03039-5 CCC: $14.00

Chart 1

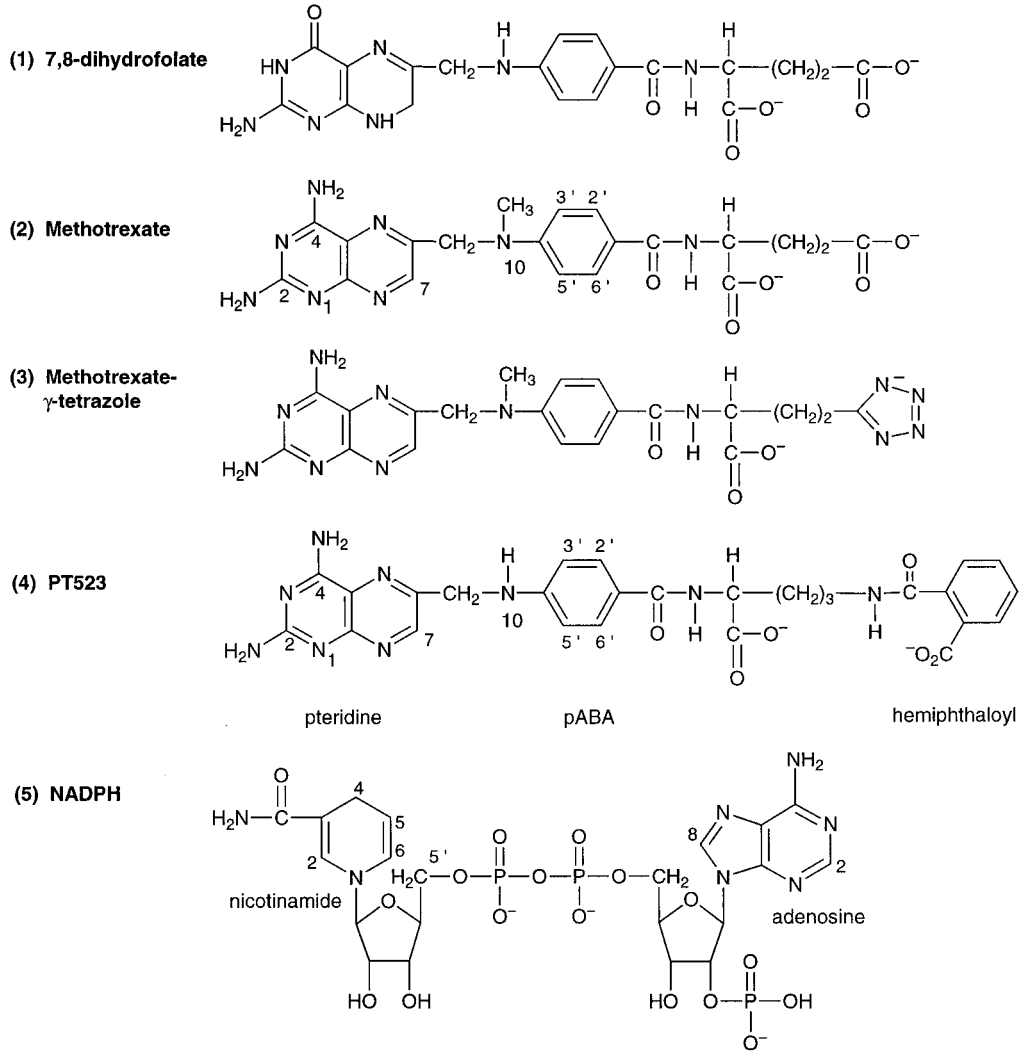

complex with NADPH and methotrexate-γ-tetrazole (MTXγT, **3**; Cody *et al.*, 1992). In addition, NMR spectroscopy has provided structure and dynamics information about DHFR−ligand complexes in solution [see Feeney *et al.* (1990), Stockman *et al.* (1991, 1992), Soteriou *et al.* (1993), Martorell *et al.* (1994), Morgan *et al.* (1995), and references therein].

MTX is a close analog of the substrate FH_2, but it binds with roughly 10^6-fold greater affinity [Appleman *et al.*, 1988; reviewed by Huennekens (1994)]. Both MTX and reduced folate are carried by active transport into the cell, where glutamates are added to their γ-carboxyl groups. Polyglutamation increases cellular retention of MTX and may also have a modest effect on binding to DHFR (Fry *et al.*, 1982; Jolivet *et al.*, 1983). The development of MTX resistance in tumor cells is a significant problem in cancer chemotherapy, and one of the main mechanisms of resistance is inefficient polyglutamation. Thus, the development of potent compounds whose efficacy is not dependent upon polyglutamation is an attractive drug-design strategy.

PT523 (**4**) is a non-polyglutamable analogue of MTX, such that the L-glutamic acid moiety of MTX has been replaced by N^{δ}-hemiphthaloyl-L-ornithine and the *N*-methyl group by N−H. The potency of PT523 is 10−100-fold higher than that of MTX against most human solid tumor cell lines (IC_{50} values of 0.1−10 nM), including several which are highly MTX-resistant (Rosowsky *et al.*, 1991, 1994; Rhee *et al.*, 1994; Chen *et al.*, 1995). Biochemical studies have suggested that the increased efficacy of PT523 may be due to stronger inhibition of DHFR, enhanced influx or hindered efflux across the cell membrane, or a combination of these effects (Westerhof *et al.*, 1995; Chen *et al.*, 1995).

We have now completed spectrophotometric enzyme inhibition studies showing that PT523 is a more potent inhibitor of human DHFR than MTX. To investigate the structural basis for the inhibition strength of PT523, 2D and 3D NMR experiments were performed on ^{15}N-labeled enzyme in the binary complex with PT523 and the ternary complex with PT523 and NADPH. Measurement of intermolecular and intramolecular NOEs, combined with restrained dynamics and energy minimization calculations, allowed the docking of PT523 and NADPH within the ligand-binding cleft of hDHFR. These studies show how small changes in ligand structure (between MTX and PT523), responsible for increased hDHFR inhibition, are correlated to structurally localized chemical shift changes and a novel binding interaction in the inhibitor−protein complex.

MATERIALS AND METHODS

Materials. MTX−agarose, FH_2, and NADPH were purchased from Sigma Chemical Co. (St. Louis, MO), and MTX was a gift of the National Cancer Institute. PT523 was

synthesized at the Dana-Farber Cancer Institute as described previously (Rosowsky *et al.*, 1988, 1989). For inhibition studies, recombinant hDHFR was expressed in *E. coli* JM107-pDFR (construct provided by Dr. Manohar Ratnam of the Medical College of Ohio, Toledo). The bacteria were grown, harvested, and processed as described by Prendergast *et al*. (1988). Recombinant hDHFR was purified to homogeneity (Kaufman, 1974), yielding approximately 80 IU of hDHFR from a 2 L culture, and characterized by gel permeation chromatography and SDS−PAGE. For NMR studies, uniformly ^{15}N-labeled hDHFR was expressed and prepared as described previously (Meiering & Wagner, 1995), except that protein was eluted from the MTX affinity column using 2 mg/mL PT523, instead of MTX, in PKEM buffer (50 mM KH_2PO_4, 52.3 mM K_2HPO_4, 50 mM KCl, 1 mM EDTA, 10 mM β-mercaptoethanol, pH 8.0). After several dilutions and reconcentrations of the samples to remove free ligand molecules, no evidence of excess ligand was seen in preliminary NMR spectra. Final NMR samples contained 2−4 mM protein complex in 25 mM KCl, 1 mM sodium azide, 50 mM potassium phosphate buffer (pH 6.5), 95% H_2O, and 5% D_2O.

hDHFR Inhibition Studies. Rates of the hDHFR-catalyzed reaction of H^+, NADPH, and FH_2, forming $NADP^+$ and FH_4 in the presence of 0 to 500 nM MTX or PT523 (50 nM increments), were determined by the method of Prendergast *et al*. (1988). A Perkin-Elmer Lambda 6 instrument with an isothermal cuvette holder was used. The temperature within the quartz cuvette (1 cm light path) was monitored independently by a NIST-traceable thermocouple. The hDHFR concentration was 235 ± 25 nM (mean ± standard deviation). Time-dependent absorbance changes were monitored at 0.1 s intervals for 4 min. When inhibitor concentrations approached stoichiometric equivalence with enzyme, initial reaction rates were followed for longer periods, up to 10 min, with proportionately longer data-collection intervals.

Concentrations of MTX, PT523, NADPH, and FH_2 were measured using UV−visible spectroscopy of the two inhibitors and the 340 and 283 nm absorbances of the cofactor (Hillcoat *et al*., 1967) and substrate (Blakley, 1969), respectively. Both MTX and PT523 were shown by HPLC to be >99% pure and stable for 72 h at 22 and 37 °C in the K_i and K_m assay buffers.

The Michaelis−Menten constant (K_m) for FH_2 was determined by the method of Delcamp *et al*. (1983), except that a water-jacketed, 5 cm path length, quartz cuvette was used in the Lambda 6 spectrophotometer, and substrate concentrations were increased in 30 nM increments from 30 to 210 nM. Inhibition constants for MTX and PT523 were obtained from the Straus and Goldstein equation for zone B inhibitors (Straus & Goldstein, 1943) by the curve-fitting method of Jackson and co-workers, as shown in Figure 1 (Jackson *et al*., 1976).

NMR Experiments. Spectra were acquired on Bruker AMX-500 or AMX-600 spectrometers with a probe temperature of 298 K except where otherwise noted. Chemical shifts were referenced to H_2O at 4.76 ppm for ^{1}H and external $^{15}NH_4Cl$ (2.9 M) in 1 M HCl at 24.93 ppm for ^{15}N. Homonuclear 2D ^{1}H experiments included NOESY (Jeener *et al*., 1979; Anil Kumar *et al*., 1980; mixing time 75 ms), TOCSY (Braunschweiler & Ernst, 1983; mixing times 56, 84, 112, and 140 ms) using a clean DIPSI-2 mixing pulse sequence (Cavanagh & Rance, 1992; Shaka *et al*., 1988), and ROESY (Bothner-By *et al*., 1984; Bax *et al*., 1985; mixing times 30 and 90 ms) with small flip angle pulses (Kessler *et al*., 1987) and 90° flanking pulses (Griesinger & Ernst, 1987) to achieve ROESY mixing. Heteronuclear ^{1}H−^{15}N experiments included 2D HSQC (Bodenhausen & Ruben, 1980), 3D NOESY-HSQC (Fesik & Zuiderweg, 1988; Kay *et al*., 1989; Marion *et al*., 1989a), and 3D HNHA (Vuister & Bax, 1993). To help distinguish bound ligand and protein (^{15}N-labeled) resonances, the 2D spectra were acquired without decoupling ^{15}N. For free PT523, 2D TOCSY (mixing times 56 and 112 ms), DQF-COSY (Piantini *et al*., 1982), and ROESY (mixing time 90 ms) experiments were performed. A gradient water-suppression scheme (Kay *et al*., 1993) was used in the NOESY-HSQC and HSQC experiments, while presaturation was employed to remove solvent signal for the other 2D experiments and the 3D HNHA. Quadrature detection in the indirect dimensions was achieved by the States−TPPI procedure (Marion *et al*., 1989b).

Data were processed using FELIX (Biosym/MSI), and linear prediction by the method of Olejniczak and Eaton (1990) was used where necessary to extend the time domain data in t_1 and t_2 by a factor of 1.5−2.0. Assignment and analysis of the spectra were performed using the XEASY software package (Bartels *et al*., 1995). NOE peaks were volume-integrated using the program Peakint (also a part of XEASY) and classified as distance restraints according to their NOESY signal intensities: strong (1.8−2.5 Å), medium (1.8−3.5 Å), and weak (1.8−5.0 Å). Conservative definitions were applied, using regions of hDHFR−PT523−NADPH with minimal chemical shift changes (distant from the binding site) for calibration. Appropriate distance corrections were added in cases where pseudoatoms were necessary.

Molecular Modeling. The heavy atom coordinates from the crystal structure of methotrexate-γ-tetrazole (MTXγT) bound to hDHFR−NADPH (Cody *et al*., 1992) were obtained from the Brookhaven database of protein structures (Bernstein *et al*., 1977) for use as a starting model for the PT523 ternary complex. MTXγT is different from MTX only in the replacement of the γ-carboxyl with an isoelectronic tetrazole ring of similar pK_a (Cody *et al*., 1992; see **2** and **3**). A model of PT523 (**4**) was built using ChemDraw (CambridgeSoft Corp.) and fit to the bound MTXγT conformation up to the shared δ-carbon. The remaining atoms of PT523, an amide linker and hemiphthaloyl ring, were set in a planar conformation, projecting away from the protein, that avoided steric clash with the δ-protons. No adjustments to hDHFR atoms were necessary, and no new binding contacts were introduced by the initial placement. Hydrogen atoms were added using the Builder module of the Insight II software package (Biosym, Ltd.), and the imidazole rings of all histidine residues were protonated. Since bound 2,4-diaminopteridine and 2,4-diaminopyrimidine inhibitors of DHFR have been shown in spectroscopic studies to be protonated at N1 [*e.g.*, Cocco *et al.* (1981), Birdsall *et al*. (1984), Appleman *et al*. (1988), and Basran *et al.* (1995)], this hydrogen atom was added to both MTXγT and PT523. Further, the 2′-phosphate of bound NADPH has been demonstrated to be dianionic in several studies [see Feeney *et al.* (1975) (*L. casei*) and Cayley *et al.* (1980) (*E. coli*)], and this modification was also made in the complexes. All structures were displayed, manipulated, and calculated using

Insight II-Discover or QUANTA-CHARMm software (MSI-Biosym) on Silicon Graphics Onyx, Indigo2 R4000, and Indigo2 R8000 computers. To remove any bad van der Waals contacts in the two initial structures, 100 steps of steepest descent minimization, followed by 100 steps of conjugate gradient minimization, were performed without restraints using Discover with a consistent valence force field (CVFF).

A restrained dynamics and energy minimization protocol [similar to those of Martorell *et al*. (1994) and Morgan *et al*. (1995)] was then carried out for hDHFR−PT523−NADPH using the NMR_Refine module of Insight II, with the CVFF force field. Harmonic NOE restraints with a 15 kcal mol^{-1} $Å^{-1}$ force constant were used throughout the protocol, and no electrostatic terms were included. The calculation began with 500 steps of minimization (100 steepest descent, 400 conjugate gradient) with the enzyme coordinates fixed, followed by 1000 steps of conjugate gradient minimization in which side chains of residues with a medium or strong NOE to any PT523 proton or within 2.5 Å of PT523 were allowed flexibility. These residues were the following: Ile 7, Leu 22, Glu 30, Phe 31, Phe 34, Gln 35, Ser 59−Pro 61, Asn 64, Leu 67, and Arg 70. A Lennard-Jones (6-12) potential with a cutoff of 10 Å was used to model the nonbond interactions. The first 300 steps of the calculation used nonbond and covalent force coefficients of 0.1, with NOE restraints set to 0.05 of their final value. The covalent and nonbond coefficients were set to 1.0 for the remaining steps, while the NOE scaling factor was gradually increased to a value of 0.3 (0.1 after step 300, 0.2 after step 500, and 0.3 after step 700).

The dynamics phase of the protocol was then performed on the minimized complex at a temperature of 300 K in four stages of 600 cycles (1 fs per cycle), for a total of 2.4 ps. The same side chains were allowed freedom as in the last phase of the preliminary minimization, and all NOE restraints were included. A quartic potential was used for the nonbond interactions to allow occasional van der Waals overlap. Scaling factors were increased in geometric increments at the end of each dynamics phase, from 0.2 to 1.0 (for nonbond and covalent forces) and from 0.3 to 1.0 (for NOE restraints) over the course of the simulation.

A final minimization series was then performed, using a Lennard-Jones potential with a 13 Å nonbond cutoff and all scaling factors set to 1.0. The restrained minimization used 500 cycles of steepest descent followed by 6000 cycles of conjugate gradient to convergence at 0.002 kcal mol^{-1} $Å^{-1}$ maximum derivative. Flexibility was allowed for the side chain and backbone atoms of residues within 3.5 Å of PT523 or NADPH after the initial minimization and those having an NOE to one of the ligand atoms. In order to allow larger adjustments of helices and loops in the complex, mobility was also given to residues in secondary structure elements which contained a large fraction of residues within 3.5 Å of PT523 or NADPH. The mobile residues were Ile 7−Ala 9, Ile 16−Thr 40, Gly 53−Asn 64, Leu 67−Arg 70, Leu 75−Glu 78, Arg 91−Leu 93, Val 115−Tyr 121, Glu 123, Thr 136, and Thr 146.

Since electrostatic forces were not included in the above protocol, an additional minimization with electrostatic terms in the energy function (200 steps steepest descent, 2000 steps conjugate gradient, constant dielectric = 1.0) was performed on the resultant structures to generate an alternative set of models for hDHFR−PT523−NADPH. All protein coordinates were fixed except for the side chains of the charged residues which were allowed flexibility during the dynamics phase. Finally, since there were no NOE restraints between hDHFR and the region of PT523 between the pABA and hemiphthaloyl rings, the simulation protocols (with and without electrostatic forces) were repeated with the addition of two distance restraints between the α-carboxylate of PT523 and the guanidinium of Arg 70 (Hη−O distances ≤2.4 Å) to model this strictly conserved ionic interaction.

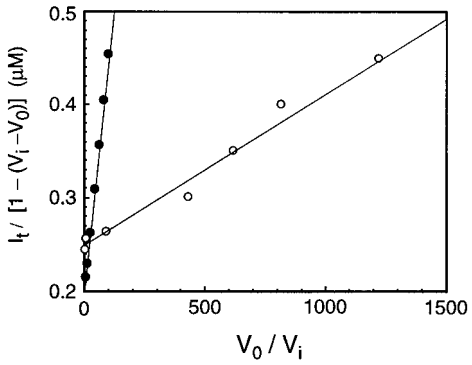

FIGURE 1: Straus−Goldstein linearization plots (Straus & Goldstein, 1943) for MTX (open circles) and PT523 (closed circles) binding to hDHFR in the presence of NADPH, where V_i and V_0 are the initial velocities in the presence and absence of inhibitors, respectively, and I_t is the total inhibitor concentration (bound + free). Data are mean values from six experiments per compound performed on different days with fresh solutions prepared daily. The homogeneous standard deviation (Bartlett's test) for the *Y*-axis data was 0.00025 μM for both inhibitors. Inhibition constants were calculated as K_i = (slope × 10^3)/[1 + (substrate concentration/K_m)] (Jackson *et al*., 1976).

RESULTS AND DISCUSSION

Inhibition Constants. The Michaelis−Menten constant (K_m) for FH_2 was found to be 100 nM, in exact agreement with that obtained by Appleman *et al*. using two other methods (1988). From the K_m and the line slopes shown in Figure 1, K_i values for MTX and PT523 (5.19 ± 0.36 and 0.35 ± 0.10 pM, respectively, mean ± 95% confidence interval) were calculated on the basis of six replicate experiments with each inhibitor. Previously reported values for the K_i of MTX against hDHFR vary with source and assay conditions and range from 3.4 to 7.3 pM [cf. Appleman *et al*. (1988)]. The approximately 15-fold lower inhibition constant of PT523 compared to MTX under these assay conditions suggests that much of the increased antitumor potency of PT523 is due to tighter binding to hDHFR.

hDHFR Resonance Assignments for the Binary Complex. Assignment of the binary complex resonances was complicated by the fact that about half of the residues in this complex had greatly broadened or doubled $^1H-^{15}N$ 2D HSQC peaks (Figure 2). Further, the NMR samples began to precipitate after several days, so a limited number of experiments could be performed. Although assignment of the doubled and often overlapping HSQC peaks was difficult, backbone amide ^{15}N and ^1H resonances could be assigned to 98% (170/174) of non-prolyl residues in the hDHFR−PT523 binary complex with the aid of ^{15}N-resolved NOESY-HSQC and HNHA spectra. The assignments for hDHFR−MTX of Stockman *et al*. (1992) were a useful guide, since the backbone chemical shifts were similar for most residues.

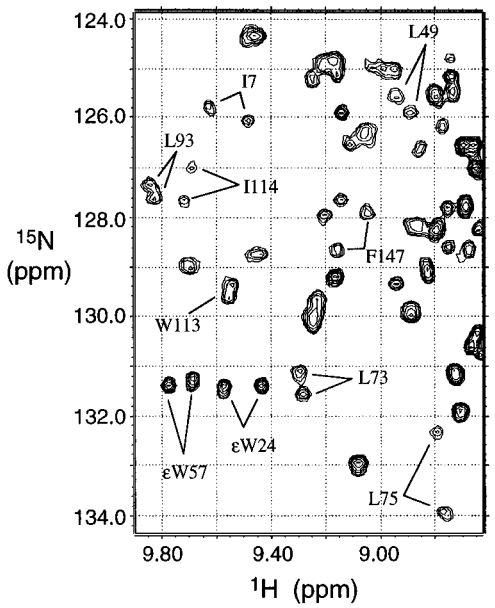

FIGURE 2: Region of the hDHFR−PT523 binary HSQC spectrum, showing that many ^{15}N−^{1}H peaks are broadened or doubled, which suggests that the complex has two bound conformations. The intensity ratio of the two resonance sets is approximately 1 to 1.15. Several assignments are shown, using single-letter amino acid abbreviations and residue numbers. Two Nε−NεH cross peaks from tryptophan side chains are also indicated.

HSQC cross peaks at similar positions were initially assumed to correspond to equivalent nuclei in the two complexes and then confirmed using NOESY-HSQC and HNHA spectra. hDHFR residues with doubled resonances are distributed throughout the enzyme, indicating widespread structural differences; however, residues around the NADPH and PT523 binding sites appear to contain a slightly higher proportion of these nuclei.

The source of the resonance splitting was investigated as follows. Titration of additional PT523 into the sample had no effect on the HSQC spectrum. Acquisition of HSQC spectra at different temperatures (283, 290.5, and 298 K) also did not have a significant effect on the splitting of the resonances. (Spectra were not acquired at higher temperatures to preserve the integrity of the samples.) Upon titrating NADPH into the sample, however, the broadened and multiplet peaks were replaced by single HSQC resonances (for 96% of hDHFR residues). These experiments suggest that the two sets of peaks observed in the binary complex are due to two conformations of hDHFR−PT523, rather than to distinct chemical species. The discovery of doubled resonances within the NADPH binding pocket raises the possibility that the second set of resonances is due to partial occupancy of this site, perhaps by another PT523 molecule or an impurity within the sample. Although we cannot rule out this occurrence, it is improbable. A second molecule of PT523 is unlikely to bind in the NADPH site because the titration of additional PT523 into the sample did not affect the relative intensity of the resonances, which would be expected if one of the species had two bound inhibitor molecules. The presence of a contaminant in the PT523 or protein sample is also unlikely, since all peaks of significant intensity in the 1D spectrum of PT523 and the 2D HSQC spectra of hDHFR−PT523−NADPH could be accounted for.

Multiple conformations have been observed previously in DHFR−ligand complexes, including *L. casei* ternary complexes with trimethoprim, folate, and pyrimethamine [Birdsall *et al.*, 1984, 1990; Cheung *et al.*, 1993; reviewed by Kraut and Matthews (1987)], but there is no evidence for multiple conformations in the hDHFR−MTX complex, with or without coenzyme (Stockman *et al.*, 1991; Meiering & Wagner, 1995). Bound to *E. coli* DHFR, however, MTX has paired resonances, while DHFR−MTX−NADPH has a single set of resonances (Falzone *et al.*, 1991; Cheung *et al.*, 1992), as is observed for PT523.

hDHFR Resonance Assignments for the Ternary Complex. Spectra of the ternary complex were much easier to assign than those of the binary complex. ^{1}H and ^{15}N assignments of the hDHFR−MTX−NADPH equivalent complex (Meiering & Wagner, 1995; E. M. Meiering, unpublished data) were again useful as a starting point. With HNHA and NOESY-HSQC data, 171 of 174 non-prolyl backbone amides and the three tryptophan NεH groups were assigned. In order to make a more detailed comparison to the spectra of hDHFR−MTX−NADPH, assignments were also obtained for 170 Hα atoms and numerous side chain atoms of hDHFR, as well as for many previously unassigned hDHFR side chain protons of the hDHFR−MTX−NADPH complex, often with the aid of ^{1}H−^{1}H TOCSY and 2D NOESY spectra. Severe overlap in the aromatic region prevented complete assignment of these side chains. Comparison of the ternary complex assignments with those of the binary complex revealed substantial ^{1}H and ^{15}N shift changes (>0.1 ppm for ^{1}H and >0.5 ppm for ^{15}N) primarily for residues near the ligand binding groove. Particularly large shift differences were found within the following residue ranges: Ile 7−Ser 11, Ile 16−Leu 22, Thr 56−Ser 59, Val 74−Leu 79, and Val 115−Tyr 121.

Comparison of Chemical Shifts to hDHFR−Methotrexate Complexes. Given that the only structural differences in PT523 relative to MTX are the absence of a methyl group at N10 and the replacement of the solvent-exposed γ-carboxylate with a longer side chain (see **2** and **4**), it is perhaps not surprising that few chemical shift differences (Δδ) were observed. Backbone chemical shift changes of the PT523 ternary complex are shown in Figure 3 relative to hDHFR−MTX−NADPH. A small number of residues, clustered together in primary sequence, show appreciable amide chemical shift differences (25 have ^{1}H shifts >0.05 ppm and 27 have ^{15}N shifts >0.20 ppm). Further, only the following 15 residues were found to have relatively large chemical shift differences (^{1}H >0.1 ppm or ^{15}N >0.5 ppm): Lys 18, Asp 21, Leu 27−Asn 29, Phe 31−Tyr 33, Gln 35, Thr 56−Ile 60, and Ser 118. Substantial Δδ values for the Hα resonances of hDHFR−PT523−NADPH are also few in number. Only five (Asp 21, Arg 28, Asn 29, Thr 56, and Leu 60) have Δδ values greater than 0.1 ppm, and all of these also have large backbone amide shift differences. The great majority of assigned side chain resonances are also unchanged from those of hDHFR−MTX−NADPH. For the most part, similar regions of the binary and ternary PT523 complexes contain chemical shift changes (relative to corresponding MTX complexes), although additional binary complex shift differences are observed in areas of hDHFR near the NADPH binding site (*e.g.*, Leu 75−Arg 77). Both binary complex conformers are likely to have structural differences from hDHFR−MTX, since chemical shift changes are observed for both sets of resonances.

Table 1: Free and Bound Ligand Resonances[a]

	atom(s)	hDHFR−PT523−NADPH	hDHFR−MTX−NADPH	bound reference shift	free ligand
PT523					
pteridine	H7	8.27	8.05	7.91[b]	8.70
	2-NH_2	12.65	12.69	10.40,[d] 6.64[d]	8.10,[d] 7.90[d]
pABA	3′,5′-H	6.13	6.20	6.15[b]	6.80
	2′,6′-H	NA	NA	7.33[b]	7.66
hemiphthaloyl[c]		6.77	−	−	7.27
		7.12	−	−	7.32
		7.48	−	−	7.42
		7.51	−	−	7.55
NADPH					
adenine	A2	7.16	7.14	7.32[f]	8.25[f]
nicotinamide	H6	6.38	6.45	6.78[e]	5.97[f]
	H5	5.70	5.78	5.56[e]	NA
	H4-2H	3.57	NA	3.50[f]	2.86[f]
ribose	H5′-2H	3.73	3.79	3.75,[e] 3.97[e]	NA

[a] ^{1}H chemical shifts are ±0.01 ppm and were measured at pH = 6.5 unless otherwise noted. A dash indicates the atom is not present, and NA means a chemical shift could not be assigned with confidence. The proton pairs of the 2-NH2, pABA, H4, and H5′ groups could have distinct chemical shifts even though only one resonance was identified. [b] Stockman *et al*., 1991; hDHFR−MTX. [c] Ring protons of the bound hemiphthaloyl moiety have not been individually assigned. They are shown here in numerical order and may not correspond to the free hemiphthaloyl assignments, since the relative order of the chemical shifts may change upon binding. [d] Basran *et al*., 1995; DHFR−MTX (*L. casei*). [e] Gerothanassis *et al*., 1992; DHFR−MTX−NADPH (*L. casei*). [f] Hyde *et al*., 1980; DHFR−MTX (*L. casei*). A 3.75 ppm correction was added to the dioxane-referenced chemical shifts.

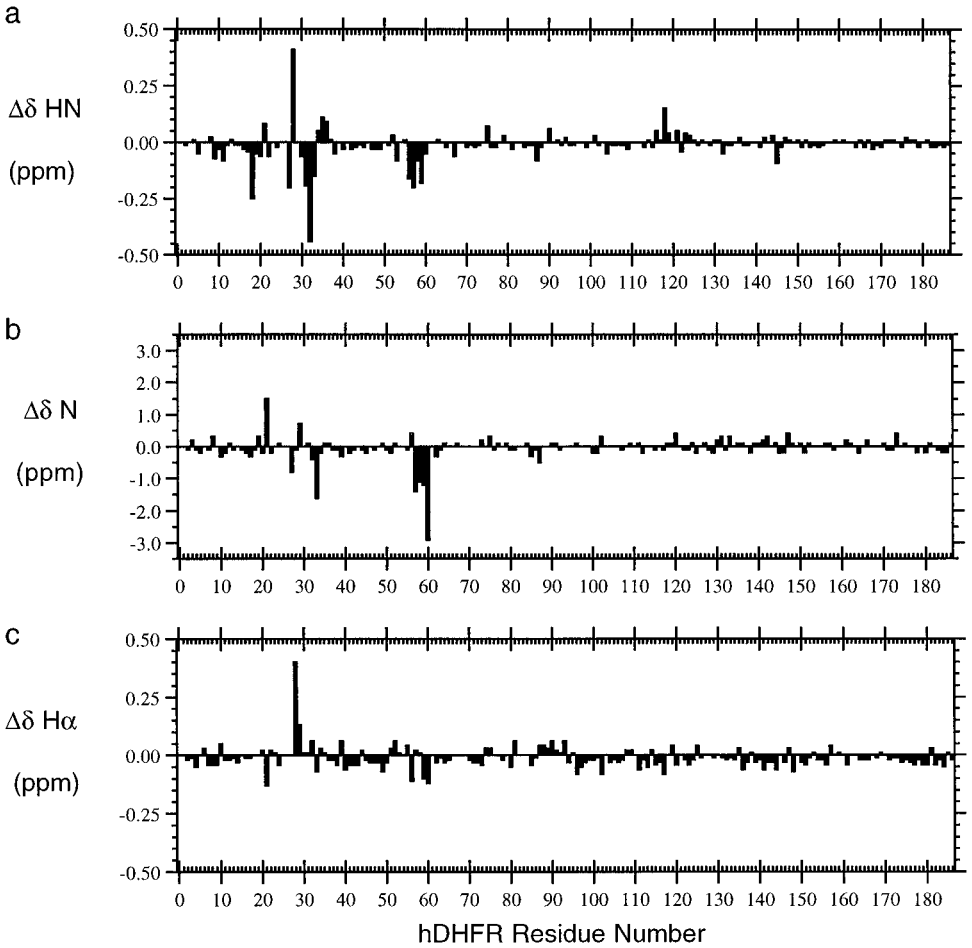

FIGURE 3: Comparison of human DHFR chemical shifts in the ternary hDHFR−PT523−NADPH and hDHFR−MTX−NADPH complexes. Chemical shift changes ($\Delta\delta$) for the backbone ^{1}H, ^{15}N, and ^{1}Hα atoms are graphed in (a), (b), and (c), respectively. The chemical shifts (ppm) of nuclei in the PT523 ternary complex nuclei were subtracted from those of equivalent nuclei in the MTX ternary complex to obtain values for $\Delta\delta$. If one or both assignments are missing [which is the case for proline residues; in (a) and (b), Val 1, Lys 54, Gly 69; and in (c), Val 1, Leu 27, Gln 35, Lys 54, Leu 67−Gly 69, Leu 79, Ser 118, and His 130], no $\Delta\delta$ value is shown. In (c), a comparison is made for only one of the two Hα protons of each glycine residue. However, the $\Delta\delta$ values of all assigned glycine Hα protons are ≤0.05 ppm.

The fact that exchanging bound MTX for PT523 resulted in minimal chemical shift changes for most hDHFR residues indicates that the protein backbone structure of these complexes is largely the same. Residues with relatively large chemical shift differences in the ternary complex were clustered mainly around three specific areas (as judged from the X-ray structure of hDHFR−MTXγT−NADPH): near N10 of the inhibitor, near the nicotinamide and nicotinamide

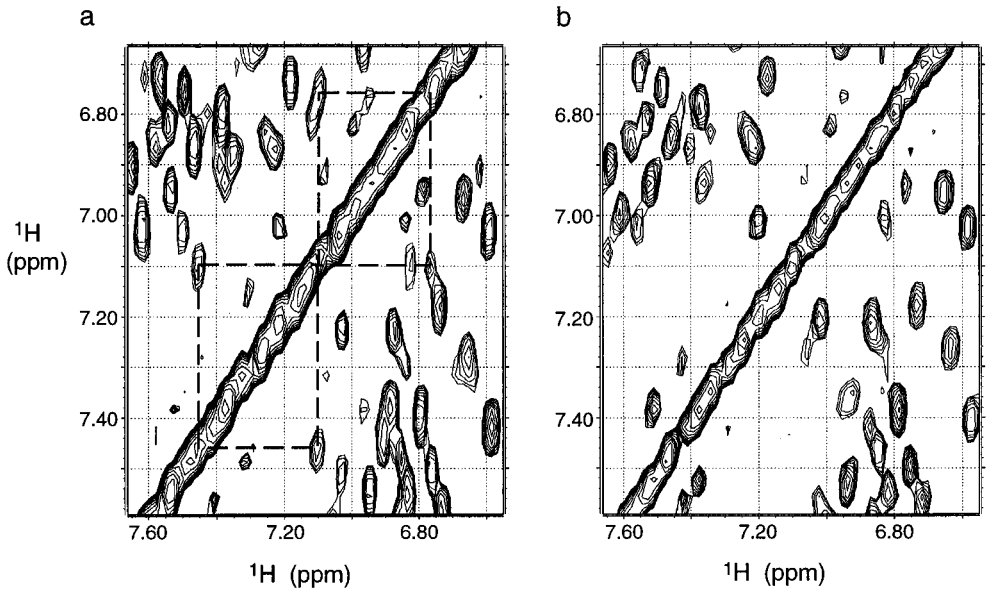

FIGURE 4: (a) Region of the ^{1}H−^{1}H NOESY spectrum of hDHFR−PT523−NADPH, showing intramolecular NOE resonances among the PT523 hemiphthaloyl ring protons. Symmetric cross peaks are indicated by dashed lines. These peaks are not observed in the same region of the MTX ternary NOESY spectrum (b).

ribose, and within the N-terminal section of the αB helix (Leu 27−Gln 35). The large $\Delta\delta$ values observed for the αB helix, which is near the hemiphthaloyl ring in the starting model of hDHFR−PT523−NADPH, strongly suggest that a new intermolecular contact is made between these substructures.

Identification of Ternary Complex Bound Ligand Resonances. Chemical shifts of ligand resonances bound to hDHFR and free in solution are given in Table 1. Free ligand resonances were assigned using ^{1}H TOCSY, ROESY, and 1D spectra. Many ligand atoms in hDHFR−PT523−NADPH were assigned using ternary MTX spectra for reference, particularly in the aromatic region where signal overlap was severe. For example, a sharp singlet at 8.27 ppm was assigned to the H7 proton of the pteridine ring system of PT523 (see **4**). The assignment of this resonance, which is not scalar coupled to other atoms, is supported by the observation of resonances with similar cross peaks in the binary MTX complex at 7.91 ppm (Stockman *et al*., 1991) and in the ternary MTX complex at 8.05 ppm. In both MTX complexes H7 also has a clear cross peak to the N10−CH_3 of MTX (assigned to 3.22 ppm in the ternary complex). The pABA 3′,5′ protons were also assigned using a cross peak to the N10−CH_3 in the MTX ternary complex. A low-field resonance at 12.65 ppm was assigned to the 2-amino group of the pteridine ring by virtue of its single set of resonances in the 2D NOESY spectrum and a cross peak to the methyl group of Ala 9. A quartet of resonances in the TOCSY spectrum for hDHFR−PT523−NADPH had no MTX analogue and was assigned to the hemiphthaloyl ring protons of PT523. This assignment was further supported by the observation of unique cross peaks among some of these nuclei in the 2D NOESY (Figure 4) and NOEs to Leu 27 and Arg 28. Because of their chemical shift similarity and overlap in the aromatic regions of the TOCSY and NOESY spectra, the resonances could not be definitively assigned to individual ring protons.

Assignment of NADPH resonances was often guided by comparison to binary hDHFR−PT523 spectra. For example, cross peaks between the adenine A2 proton and the amide protons of Ser 76 and Arg 77 are present only in the ternary NOESY-HSQC. The H5 and H6 atoms of the NADPH nicotinamide have a TOCSY cross peak and several NOE connections to neighboring protein atoms. NOESY cross peaks between nicotinamide H4 and H5 protons and between H5′ of the nicotinamide ribose and H6 allowed these atoms to be assigned as well.

Ternary Complex NOEs. The intermolecular NOEs used for structure calculations are depicted in schematic form in Figure 5. Ligand intramolecular NOEs (not shown) were observed for H4−H5, H4−H6, and H6−H5′ of NADPH and among the hemiphthaloyl ring protons of PT523 (Figure 4). To restrict and define the conformation of residues in the ligand-binding region of hDHFR, an additional 149 protein−protein NOEs were used. Emphasis was placed upon finding NOEs among residues nearest the inhibitor and cofactor, particularly longer range constraints definitive of the local protein conformation. Many protein−ligand NOEs were identified first as HN cross peaks in the 3D NOESY-HSQC spectrum and then in the more-crowded 2D NOESY. If the strength of a peak was ambiguous because of signal overlap, it was classified as weak. The hDHFR−MTX−NADPH spectra, including a NOESY-HSQC spectrum of the hDHFR mutant E30A (Meiering & Wagner, 1995), were again useful for sorting out cases of signal overlap, and the MTXγT ternary crystal structure was occasionally consulted to verify the plausibility of NOE assignments. The set of NOEs between the aromatic ring protons of Phe 31 and the H7 proton of PT523 is shown is Figure 6. Only a few, weak NOEs could be found for the hemiphthaloyl group of PT523. This could be due to the crowded NOESY spectra and the large number of unassigned proline residues (23, 25, and 26) near this group. It might also indicate, however, thatthe hemiphthaloyl ring is not tightly bound in one conformation. Most intermolecular NOEs for the NADPH cofactor involve the nicotinamide ring, where clear intramolecular connectivities simplified resonance assignment. Figure 7 shows the NOEs for H5 and H6 of the nicotinamide ring with the HN protons of Gly 117 and Ser 118 in the NOESY-HSQC.

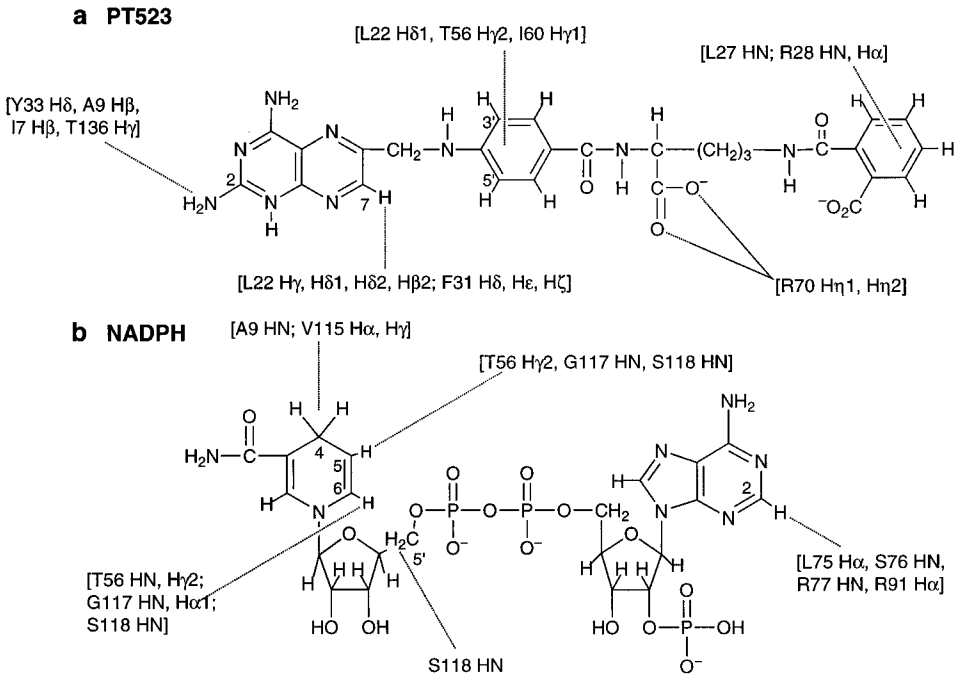

FIGURE 5: Schematic drawing of NOE and other restraints (a) between hDHFR and PT523 and (b) between hDHFR and NADPH, used in the restrained dynamics and minimization protocol. The restraint from Arg 70 to the α-carboxyl of PT523 is the only one not derived from a measured NOE (see text).

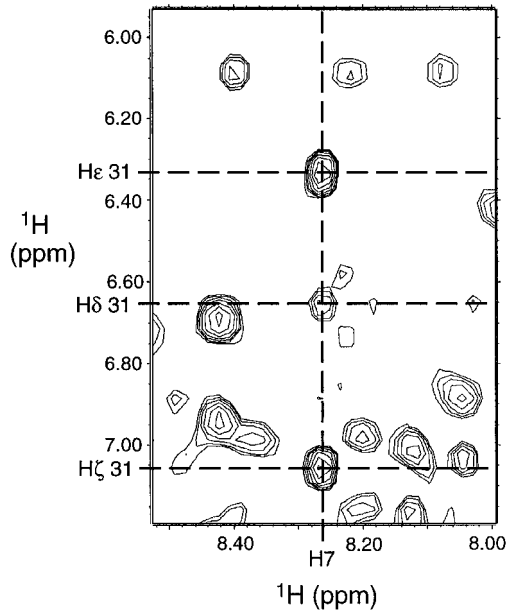

FIGURE 6: Section of the ^{1}H−^{1}H NOESY spectrum of the hDHFR−PT523−NADPH complex containing the intermolecular NOE cross peaks between H7 of the PT523 pteridine moiety and the aromatic ring protons of Phe 31.

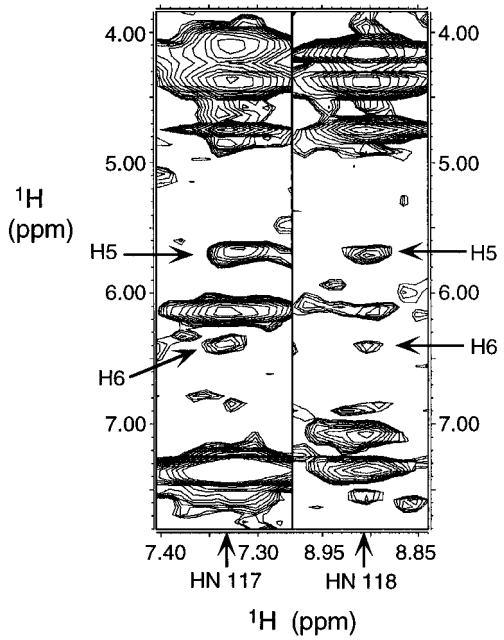

FIGURE 7: Selected slices from the ^{1}H−^{15}N NOESY-HSQC spectrum of hDHFR−PT523−NADPH, in the ^{15}N planes of Gly 117 (left, ^{15}N δ = 111.7 ppm) and Ser 118 (^{15}N δ = 120.0 ppm), showing weak HN cross peaks with H5 and H6 of the nicotinamide ring of NADPH.

Intermolecular NOEs were very similar in hDHFR−PT523−NADPH and hDHFR−MTX−NADPH. Correlates were found for all matching protein−ligand NOEs where assignments could be made, except for the cross peak between H5 (nicotinamide) and HN of Ser 118, which had a weak signal in the PT523 NOESY spectrum. The line shapes and strengths of the NOEs were also approximately the same, although overlapping signals prevented comparison in some cases. In particular, the nicotinamide H4 resonance signal in the hDHFR−MTX−NADPH spectrum appears to be overlapped with one or more peaks and thus could not be assigned or measured with confidence.

Structure Calculations. The X-ray structure of hDHFR−MTXγT−NADPH (Cody *et al.*, 1992) was used as a model for the starting structure of the restrained minimization and dynamics protocol. Justification for using this structure as a model for the MTX and PT523 ternary complexes is as follows. First, the conformation of the MTXγT inhibitor is very similar to that of MTX in bacterial DHFR structures [*e.g.*, Bolin *et al.* (1982)] and to structures of hDHFR bound to folate (Oefner *et al.*, 1988; Davies *et al.*, 1990). The tetrazole ring of MTXγT (see **3**), which projects away from the binding pocket of hDHFR, is highly solvent-exposed and

does not interact directly with the enzyme. The isosteric and isoelectronic γ-carboxylate of MTX (see **2**), which it replaces, also interacts weakly or not at all with the enzyme in related crystal structures, indicating that this difference does not significantly affect the bound conformation of MTX and MTXγT (Cody *et al*., 1992). Further, competitive inhibition assays on the two compounds with isolated and intracellular DHFR show that they have equal inhibition potency (McGuire *et al*., 1990). This biochemical and structural evidence indicates that MTXγT and MTX are likely to bind very similarly. Strong indication that PT523 should have a bound conformation similar to these inhibitors is provided by the NMR chemical shift comparisons discussed previously. The observation that only 15 residues have ^{15}N, HN, or Hα chemical shift differences greater than 0.1 ppm for ^{1}H and 0.5 ppm for ^{15}N indicates that the chemical environment of the backbone of hDHFR is virtually constant for MTX and PT523 complexes, except in a few isolated regions. More specific evidence is given by the above comparison of NOEs, which positions the pteridine and pABA groups near equivalent enzyme protons in the two complexes.

PT523 was placed in the bound conformation of MTXγT as described in Materials and Methods. Since the initial orientation of the hemiphthaloyl ring was arbitrary, it was important to ensure that it could sample alternative conformations during the dynamics phase of the simulated annealing. Examination of several dynamics trajectories confirmed that the ring was able to move freely and sample different rotational conformations during the early stages of the simulation (when the NOE scaling factor was small). Preliminary assessment of the structures generated by the protocol without electrostatic forces and without the additional Arg 70 restraint (see Materials and Methods) showed good structural convergence for the pteridine and nicotinamide rings (RMSD = 0.29 Å). The conformation of these groups was very similar to that of the hDHFR−MTXγT−NADPH crystal structure, and no ring protons of these groups had restraint violations >0.2 Å. However, the limited number of restraints to the hemiphthaloyl side chain often allowed the pABA and hemiphthaloyl groups to escape from the binding pocket during the dynamics phase, producing significant restraint violations for these groups. To help to retain the inhibitor in the binding pocket of hDHFR, the conserved Arg 70 to α-carboxylate ionic interaction was modeled as a pair of distance restraints, holding the carboxylate oxygen atoms within range for weak hydrogen bonds ($\leq$2.4 Å) to the Hη protons of Arg 70. Since electrostatic terms were not included in the energy function, this ionic interaction would not otherwise be represented.

Although the addition of this restraint biases the simulation toward a subset of conformations, there is convincing evidence that the interaction takes place in hDHFR−PT523−NADPH. This arginine is strictly conserved among DHFRs from different organisms (Arg 57 in *E. coli* and *L. casei*), and it is consistently observed in crystal structures to make two charge-mediated hydrogen bonds to the α-carboxylate of folate and folate analogue inhibitors (Kraut & Matthews, 1987), including MTX (Bolin *et al*., 1982), MTXγT (Cody *et al*., 1992), and 5-deazafolate (Davies *et al*., 1990; Reyes *et al*., 1995). The importance of this interaction for the binding of MTX was demonstrated in a study of the R70K hDHFR mutant, which binds MTX with 20 000-fold lower affinity (Thompson & Freisheim, 1991), as well as in other studies (Vehar & Freisheim, 1976; Cocco *et al*., 1977). Arg 70 lies near the protein surface but is confined by neighboring aliphatic side chains within a narrow, otherwise hydrophobic pocket. No anionic enzyme residue is close enough to supply an alternative electrostatic interaction (although the guanidinium is solvent accessible in the absence of substrate or inhibitor).

Table 2: Ligand RMSD Values for the 33 Final Structures[a]

molecule/moiety	RMSD (Å)	molecule/moiety	RMSD (Å)
all atoms		ring atoms	
PT523[b]	1.5	hemiphthaloyl[b]	1.9
NADPH	1.7	nicotinamide	0.26
ring atoms		nicotinamide ribose	0.35
pteridine	0.55	adenine ribose	1.5
pABA	0.88	adenine	1.9

[a] Regions of hDHFR which were fixed during the annealing protocol were used to align the structures. [b] Includes variance of both hemiphthaloyl ring rotamers present in the final structures.

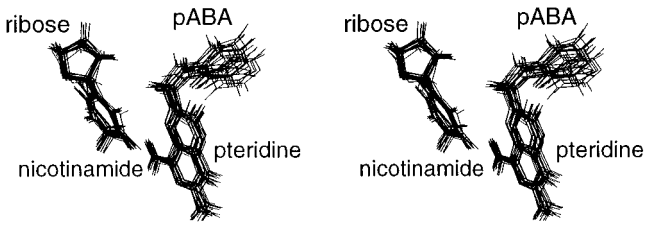

FIGURE 8: Stereo image of the superposition of the 20 lowest energy structures produced by the restrained dynamics and energy minimization protocol. Shown are the nicotinamide and ribose rings of NADPH and the pABA and pteridine rings of PT523. The adenine, diphosphate, and amide groups of NADPH and the hemiphthaloyl group of PT523 were not well constrained by NOEs and are not shown.

NMR data also indicate that PT523 has the same interaction with Arg 70 as MTX. Backbone chemical shifts for residues in the vicinity of Arg 70 (Gln 35−Thr 40, Val 50, Leu 67−Asn 72) are virtually unchanged from the MTX complex (see Figure 3). In addition, the Nϵ and NϵH nuclei of Arg 70 have well-resolved resonance signals at 86.8 and 5.72 ppm, respectively. NOEs were also found from the NϵH proton to the HN protons of Lys 68 and Arg 70. Similar chemical shifts and NOEs with similar intensities are seen in the MTX binary and ternary complexes, indicating that PT523 is likely to adopt a conformation and contacts similar to MTX in the region around Arg 70, including the conserved ionic interaction.

Using the α-carboxyl−Arg 70 restraint in addition to the NOE restraints shown in Figure 5, 60 structures of the ternary complex were generated using the dynamics and minimization protocol; 78% of these converged to 0.002 kcal mol^{-1} Å^{-1} maximum derivative. Of these 47 structures, 33 have no DHFR−ligand restraint violations $\geq$0.1 Å and no protein−protein restraint violations $\geq$0.2 Å. Table 2 contains RMSD values for various parts of PT523 and NADPH in the final set of solution structures. The PT523 pteridine and NADPH nicotinamide rings of the ligands are well defined (see Figure 8) and have the same approximate conformation with or without the Arg 70 restraint. The positions of the pABA ring of PT523 and the nicotinamide ribose also show good structural convergence in the final set of structures (Figure 8, Table 2). The combined RMSD of the ligand groups buried more deeply in the binding cleft of

hDHFR−nicotinamide, nicotinamide ribose, pteridine, and pABA−is 0.59 Å (for ring atoms). The majority of hDHFR−ligand NOEs also involve these groups. Although PT523 remains in the binding pocket with no significant restraint violations in the final structures, the hemiphthaloyl ring adopts a range of positions (RMSD = 1.9 Å).

3In order to suggest possible interactions for charged protein side chains with ligand charged and polar groups, a final NOE-restrained minimization with electrostatic terms was performed on the set of structures, allowing only the ligands and charged protein side chains to move. This additional minimization negligibly changed the bound conformation of the ligands but revealed several possible electrostatic interactions involving the hemiphthaloyl ring. Except where specifically noted, the following analysis of the bound structure will refer to results obtained without the final electrostatic minimization.

Structure of the Binding Site. (A) Inhibitor Conformation and Contacts to hDHFR. The hDHFR−MTXγT−NADPH crystal structure (Cody *et al.*, 1992) with added hydrogen atoms (see Materials and Methods) was used to make direct structural comparisons with the hDHFR−PT523−NADPH solution structure. The pteridine and pABA rings adopt orientations in the PT523 ternary complex very similar to those of MTXγT in the crystal structure, and contacts from these groups to neighboring residues are generally maintained. For example, the pABA ring remains in position to make hydrophobic contact to the Ile 60 side chain. Some variability is observed in the angular orientation of the pABA ring in the solution structures, suggesting that it may have rotational flexibility in the hDHFR−PT523−NADPH complex. Rapid flipping of the pABA ring is consistent with observation of only one resonance for the 3′,5′ protons.

The hemiphthaloyl group makes hydrophobic contacts in most of the final structures with Pro 26, Phe 31, and the α and β protons of Arg 28, a set of interactions which the shorter molecule, MTX, cannot provide (see Figure 9). The hemiphthaloyl ring face appears to pack consistently onto a hydrophobic "shelf" formed by these residues (Figure 9), but there is considerable variation in the ring position upon the shelf (RMSD = 1.9 Å). In particular, the ring adopts both *cis* and *trans* orientations relative to the adjacent amide group. In recent crystallographic studies of hDHFR−PT523−NADPH, the hemiphthaloyl ring also adopts two orientations, different by 180° rotation, plus a third orientation somewhat different from these (V. Cody, personal communication). The fact that the hemiphthaloyl group of PT523 appears able to bind in more than one rotational conformation in both the solution and crystal structures suggests that this exchange may be a real process in solution and may also explain why only a few, weak NOEs to the hemiphthaloyl ring could be found. Failure to see the third crystal conformation by NMR does not exclude the existence of this form in solution. It is also possible, however, that this conformation is present only in the crystallized complex, in which the hemiphthaloyl ring is positioned next to the packing interface between crystal monomers (V. Cody, personal communication). If the hemiphthaloyl ring is in exchange between multiple conformations, it is likely to be fast exchange for two reasons. First, only one set of hemiphthaloyl ring resonances was found; and second, the Phe 31 aromatic ring, which forms part of the shelf upon which the hemiphthaloyl ring packs, also appears to be flipping rapidly, since single resonances were observed for its δ and ϵ protons.

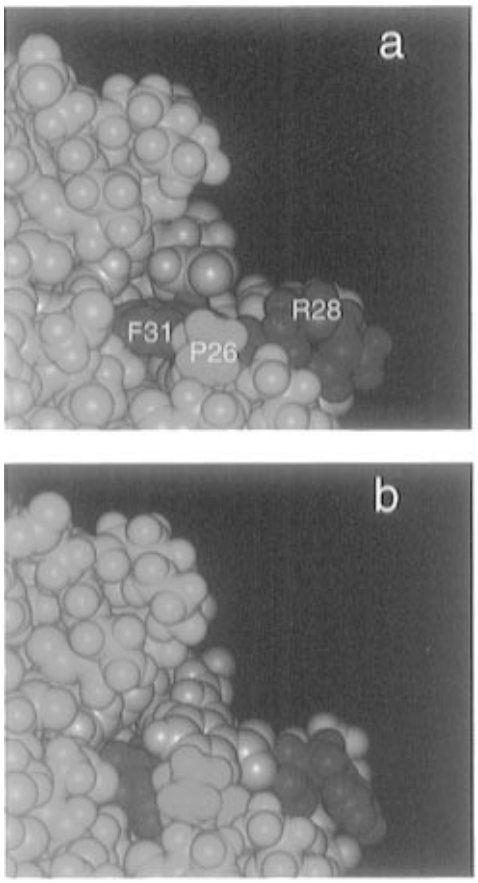

FIGURE 9: Solid-sphere van der Waals models of the inhibitors (in gray) MTX (a) and PT523 (b) bound to hDHFR, showing the hydrophobic shelf (formed by F31, P26, and R28) which interacts with the PT523 hemiphthaloyl ring in the solution structures. Four hDHFR residues which contact the hemiphthaloyl ring in many structures are shown in purple and green (Arg 32, green, is in the background), and the rest of hDHFR is shown in cyan. The terminal portions of the inhibitors protrude from the solvent-exposed opening of the binding pocket, whereas the pteridine, pABA, and α-carboxylate moieties are more deeply buried. The MTX model (a) was created from the hDHFR−MTXγT−NADPH crystal structure (Cody *et al.*, 1992), by fitting MTX to the bound conformation of MTXγT. A representative solution structure of bound PT523 (b) shows one set of possible contacts between the hemiphthaloyl group and the hDHFR shelf. DHFR backbone atoms of the two models were superimposed to align the figures.

In principle, the presence of multiple inhibitor conformations could also result in doubled or broadened resonances of hDHFR nuclei. A few residues near the hemiphthaloyl ring have broader than average backbone resonances; Leu 27, in particular, appears to have a very broad $^{1}H-^{15}N$ HSQC peak. However, the resonances of these residues do not appear substantially different from their counterparts in the hDHFR−MTX−NADPH spectra. In addition, given the high density of prolines in this region of hDHFR (residues 23, 25, and 26), the split resonance of Leu 27 could also be due to proline *cis*−*trans* isomerization.

Possible protein interactions with charged groups of PT523 were identified by examining the structures after minimization with electrostatic forces. The terminal COO− of PT523 appears to be able to form hydrogen bonds to hDHFR more easily than the γ-carboxylate of MTX, since the group extends farther from the rest of the ligand, toward several

charged and polar protein groups. For instance, the Nϵ of Arg 32 is close enough to donate a hydrogen bond in several of the final structures, and the charged side chains of Arg 28 and Lys 173 are also close to the ring carboxylate (3−5 Å) in many structures. Solvent-mediated interaction with one or more of these three residues is likely, depending on the orientation of the hemiphthaloyl ring. Additionally, the pair of hydrogen bonds observed in hDHFR−MTXγT−NADPH between the Glu 30 carboxylate and the pteridine 2-NH_2 group of MTXγT is also observed in the hDHFR−PT523−NADPH solution structures.

(B) NADPH Conformation and Contacts to hDHFR. The positions of the nicotinamide and ribose rings are also similar to those of hDHFR−MTXγT−NADPH. For example, the glycosidic bond is in the *anti* conformation, and the nicotinamide ring face packs against the pteridine ring system of PT523. One appreciable change from the MTXγT complex is a rotation of the ribose ring toward Thr 56, Ser 59, and 10H of PT523 (approximately 1 Å for C3′ and 0.5 Å for C2′), as well as a small accompanying movement of the nicotinamide ring in the same direction. A plausible explanation for these movements is to fill in the space created by the removal of the 10-CH_3 group of MTXγT. The Thr 56 and Ile 60 side chains also appear to have made packing adjustments due to the CH_3 removal. It should be noted that the ribose ring is not well constrained by NOEs, so it is possible that solvent molecules could limit this rotation and occupy some of the new space. A bound water molecule has been observed near this position in the *E. coli* crystal structure of DHFR−FH_2−$NADP^+$ (Bystroff *et al*., 1990). However, the presence of significant chemical shift changes near the ribose ring indicates that some structural change occurs in this region.

Relationship of K_i to PT523−hDHFR Contacts. It is likely that interactions made by the N^{δ}-hemiphthaloyl-L-ornithine group of PT523 make a substantial contribution to the lower K_i value of PT523. The importance of the hemiphthaloyl ring to the cytotoxicity of PT523 has been directly investigated by testing analogues of PT523 with the terminal carboxyl moiety in the *meta* and *para* positions on the ring. Structure−activity studies (A. Rosowsky, C. Vaidya, H. Bader, J. E. Wright, and B. Teicher, in preparation) have shown that a shift of the *ortho* carboxyl group of the hemiphthaloyl ring to the *meta* and *para* positions results in compounds which are 10- and 240-fold less cytotoxic, respectively, than PT523 in a clonogenic assay against a human tumor cell line. Earlier studies have shown a proportional relationship between stability of the inhibition complex and antifolate cytotoxicity, other factors (such as cellular transport) being equal (Sirotnak *et al*., 1980, 1981). These data are consistent with the solution structures which indicate potentially unfavorable steric interactions between such substituents, particularly a *para* substituent, and Pro 26 or Arg 28 (see Figure 9). Thus, the sensitivity of inhibitor cytotoxicity to the position of the ring carboxylate indicates that the observed contacts of the hemiphthaloyl ring to hydrophobic enzyme side chains may enhance the stability of the complex in solution. The only other structural variation between PT523 and MTX is at the N10 position. This difference probably has a minimal effect on binding because the removal of the MTX N10-methyl group (resulting in the antifolate drug aminopterin—a hybrid of MTX and PT523) does not significantly affect the level of DHFR inhibition (DeGraw *et al*., 1982).

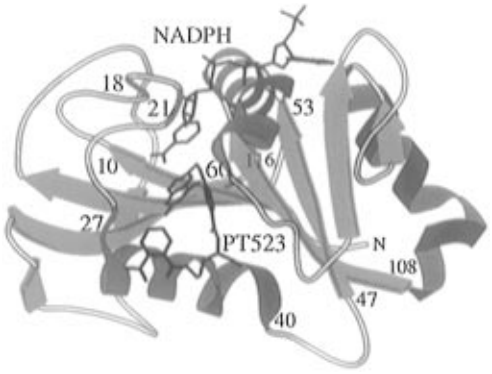

FIGURE 10: Diagram of a representative solution structure of hDHFR−PT523−NADPH, showing chemical shift changes relative to the hDHFR−MTX−NADPH complex (see also Figure 3). hDHFR is shown as a ribbon (α-helices in blue, β-strands in cyan, and coil in white), and ligands are shown using stick representation. The polyproline (II) helix comprising residues 21−26 is depicted as coil. Segments of hDHFR which contain residues with substantial chemical shift changes ($\Delta\delta$ for ^1H > 0.1 ppm or $\Delta\delta$ for ^{15}N > 0.5 ppm) are colored red. These 15 residues (Lys 18, Asp 21, Leu 27−Asn 29, Phe 31−Tyr 33, Gln 35, Thr 56−Ile 60, and Ser 118) are clustered close to the hemiphthaloyl ring of PT523 and around H10 of PT523 and the nicotinamide ribose, near the inhibitor−cofactor interface. The beginning and end of several secondary structure elements, as well as residues 18 and 21 (in red), are labeled by residue number. The figure was created using MOLSCRIPT (Kraulis, 1991).

Comparison of Structural Changes to Chemical Shift Changes. The three areas of hDHFR with the greatest chemical shift differences between the MTX and PT523 ternary complexes are also the areas which contain the greatest structural differences (Figure 10). The B helix (Leu 27−Thr 40) extends beneath the hemiphthaloyl moiety of PT523 and includes Phe 31 and Arg 28 which may contact the ring directly. Seven of the nine N-terminal residues of this helix, Leu 27−Asn 29, Phe 31−Tyr 33, and Gln 35, have relatively large backbone chemical shift changes (^1H >0.1 ppm or ^{15}N >0.5 ppm). The other residues with relatively large backbone $\Delta\delta$ values lie near the interface between PT523 and NADPH, either near N10 (Thr 56−Ile 60) or near the nicotinamide ribose (Lys 18, Asp 21, and Ser 118).

Reasonable structural interpretations can be made for many of the large chemical shift differences. The amide NH and N atoms of Arg 28, for example, are <3.5 Å from the hemiphthaloyl ring in most structures, and the NH protons of Leu 27 and Phe 31 are close enough to the aromatic ring of Phe 31 (3−4 Å) to be affected by shifts in orientation of the ring as it packs against the hemiphthaloyl group of PT523. The Hα proton of Arg 28 has the greatest observed $\Delta\delta$ for any Hα atom (0.40 ppm) and lies very close to the hemiphthaloyl ring (typically <3 Å) in the final set of structures. The Hβ protons of Phe 31 are also near the hemiphthaloyl ring (about 2.5−3.5 Å from the nearest ring carbon atom) and likewise appear in NMR data to have an altered chemical environment. In hDHFR−MTX−NADPH spectra, these protons share a single, broad resonance at 2.95 ppm, whereas in hDHFR−PT523−NADPH they are split into two distinct signals at 2.77 and 3.16 ppm. Ring shift currents associated with the hemiphthaloyl group as well as structural adjustments in the αB helix as it interacts with the ring supply plausible explanations for the shift changes

mentioned above. In the MTXγT ternary complex, Lys 18 and Asp 21 share a pair of backbone hydrogen bonds (the NH of each to the CO of the other). The large $\Delta\delta$ values for these two NH groups suggest that these bonds may be disrupted by structural adjustments near the ribose ring. (The backbone N of Asp 21 is <4.0 Å from the ribose in all structures.) This region of the protein is one of the most variable in the set of solution structures, and while the variability is consistent with the interpretation that one or more of these bonds may be disrupted, it also prevents prediction of new hydrogen-bonding relationships.

In the same way that regions of the PT523 ternary complex with larger chemical shift differences relative to hDHFR−MTX−NADPH appear to undergo larger structural changes, regions without appreciable $\Delta\delta$ values generally have minimal structural differences. The correlations between chemical shift and structure support the NOE-based structural model of the binding of PT523 to human DHFR and offer insight into the changes in chemical environment associated with modified ligands. To further refine the structure, additional NOEs to the hemiphthaloyl and L-ornithine groups of PT523 are necessary. These might be obtained through assignment of nearby proline residues and other side chain protons, which could be possible with NMR experiments on $^{13}C-^{15}N$, doubly labeled hDHFR. The existence and occupancy of different conformational states of the hemiphthaloyl ring could be further analyzed by rotating frame relaxation experiments (Deverell *et al*., 1970). Future work may also include NMR studies of the hDHFR−aminopterin−NADPH complex to ascertain whether the two sets of changes in chemical shift and structure seen in the PT523 complex, associated with the removal of the N10−CH_3 and the addition of the hemiphthaloyl group, are independent.

Conclusions. Two conformational states in slow exchange were observed for the binary hDHFR−PT523 complex, in contrast to the single state for hDHFR−MTX (Stockman *et al*., 1991) and the PT523 ternary complex. The regions exhibiting the greatest backbone chemical shift differences between hDHFR−MTX−NADPH and hDHFR−PT523−NADPH also have the largest structural differences; these are situated near the hemiphthaloyl group of PT523 and around the interface between PT523 and NADPH. Many of these chemical shift differences have plausible structural explanations. In the calculated solution structures of the ternary complex, the hemiphthaloyl group of PT523 extends from the folate binding pocket to contact a hydrophobic shelf formed by N-terminal residues of the αB helix. The presence of multiple hemiphthaloyl ring conformations is consistent with both solution NMR and crystallographic studies (V. Cody, personal communication). Contacts between the hemiphthaloyl group and hDHFR, which are not possible in hDHFR−MTX−NADPH, offer a structural explanation for the superior inhibition potency of PT523.

ACKNOWLEDGMENT

The authors acknowledge Dara Gilbert for helpful discussions, Johnathan Choi for assistance with the XEASY software package, and Vivian Cody for communication of unpublished results.

SUPPORTING INFORMATION AVAILABLE

A list of ^{1}H and ^{15}N backbone sequential resonance assignments for the binary hDHFR−PT523 complex compared to those of hDHFR−MTX, a table of assigned backbone and side chain hDHFR chemical shifts in the ternary complex with PT523 and NADPH, and lists of hDHFR−ligand and ligand intramolecular NOE restraints, and hDHFR intramolecular NOE restraints, used in the dynamics and energy minimization protocol (10 pages). Ordering information is given on any current masthead page.

REFERENCES

Anil Kumar, Ernst, R. R., & Wüthrich, K. (1980) *Biochem. Biophys. Res. Commun. 95*, 1−6.

Appleman, J. A., Prendergast, N., Delcamp, T. J., Freisheim, J. H., & Blakley, R. L. (1988) *J. Biol. Chem. 263*, 10304−10313.

Bartels, C., Xia, T.-H., Billeter, M., Güntert, P., & Wüthrich, K. (1995) *J. Biomol. NMR 5*, 1−10.

Basran, J., Casarotto, M. G., Barsukov, I. L., & Roberts, G. C. K. (1995) *Biochemistry 34*, 2782−2882.

Bax, A., & Davis, D. G. (1985) *J. Magn. Reson. 63*, 207−213.

Bernstein, F. C., Koetzle, T. F., Williams, G. J. B., Meyer, E. F., Brice, M. D., Rodgers, J. R., Kennard, O., Shimanouchi, T., & Tasumi, M. (1977) *J. Mol. Biol. 112*, 535−542.

Birdsall, B., Bevan, A. W., Pascual, C., Roberts, G. C. K., Feeney, J., Gronenborn, A., & Clore, G. M. (1984) *Biochemistry 23*, 4733−4742.

Birdsall, B., Tendler, J. B., Arnold, R. P., Feeney, J., Griffin, R. J., Carr, M. J., Thomas, J. A., Roberts, G. C. K., & Stevens, M. F. G. (1990) *Biochemistry 29*, 9660−9667.

Blakley, R. L. (1969) in *The Biochemistry of Folic Acid and Related Pteridines*, p 93, Elsevier Press, New York.

Blakley, R. L. (1984) in *Chemistry and Biology of Folates, Vol. I: Folates and Pterins* (Blakley, R. L., & Benkovic, S. J., Eds.) Vol. 1, Chapter 5, pp 191−253, J. Wiley, New York.

Blakley, R. L. (1995) *Adv. Enzymol. 70*, 23−102.

Bodenhausen, G., & Ruben, D. J. (1980) *Chem. Phys. Lett. 69*, 517−552.

Bolin, J. T., Filman, D. J., Matthews, D. A., Hamlin, R. C, & Kraut, J. (1982) *J. Biol. Chem. 257*, 13650−13662.

Bothner-By, A. A., Stephens, R. L., Lee, J.-M., Warren, C. D., & Jeanloz, R. W. (1984) *J. Am. Chem. Soc. 106*, 811−813.

Braunschweiler, L., & Ernst, R. R. (1983) *J. Magn. Reson.* 53, 521−528.

Bystroff, C., Oatley, S. J., & Kraut, J. (1990) *Biochemistry 29*, 3263−3277.

Cavanagh, J., & Rance, M. (1992) *J. Magn. Reson. 96*, 670−678.

Cayley, P. J., Feeney, J., & Kimber, B. J. (1980) *Int. J. Biol. Macromol. 2*, 251−255.

Chen, G., Wright, J. E., & Rosowsky, A. (1995) *Mol. Pharmacol. 48*, 758−765.

Cheung, H. T., Birdsall, B., & Feeney, J. (1992) *FEBS Lett. 312*, 147−151.

Cheung, H. T. A., Birdsall, B., Frenkiel, T. A., Chau, D. D., & Feeney, J. (1993) *Biochemistry 32*, 6846−6854.

Cocco, L., Blakley, R. L., Walker, T. E., London, R. E., & Matwiyoff, N. A. (1977) *Biochem. Biophys. Res. Commun. 68*, 937−941.

Cocco, L., Groff, J. P., Temple, C., Jr., Montgomery, J. A., London, R. E., Matwiyoff, N. A., & Blakley, R. L. (1981) *Biochemistry 20*, 3972−3978.

Cody, V., Luft, J. R., Ciszak, E., Kalman, T. I., & Freisheim, J. (1992) *Anti-Cancer Drug Design 7*, 483−491.

Davies, J. F., Delcamp, T. J., Prendergast, N. J., Ashford, V. A., Freisheim, J. H., & Kraut, J. (1990) *Biochemistry 29*, 9467−9479.

DeGraw, J. I., Brown, V. H., Tagawa, H., Kisliuk, R. L., Gaumont, Y., & Sirotnak, F. M. (1982) *J. Med. Chem. 25*, 1227−1230.

Delcamp, T. J., Susten, S. S., Blankenship, D. T., & Freisheim, J. H. (1983) *Biochemistry 22*, 633−639.

Deverell, C., Morgan, R. E., & Strange, J. H. (1970) *Mol. Phys. 18*, 553−559.

Falzone, C. J., Wright, P. E., & Benkovic, S. J. (1991) *Biochemistry 30*, 2184−2191.

Feeney, J. (1990) *Biochem. Pharmacol. 40*, 141−152.

Feeney, J., Birdsall, B., Roberts, G. C. K., & Burgen, A. S. V. (1975) *Nature 257*, 564−566.
Fesik, S. W., & Zuiderweg, E. R. P. (1988) *J. Magn. Reson. 78*, 588−593.
Freisheim, J. H., & Matthews, D. A. (1984) in *Folate Antagonists as Chemotherapeutic Agents* (Sirotnak, F. M., Burchall, J. J., Ensminger, W. D., & Montgomery, J. A., Eds.) Vol. 1, pp 69−131, Academic Press, Orlando, FL.
Fry, D. W., Yalowich, J. C., & Goldman, I. D. (1982) *J. Biol. Chem. 257*, 1890−1896.
Gerothanassis, I. P., Birdsall, B., Bauer, C. J., & Feeney, J. (1992) *Eur. J. Biochem. 204*, 173−177.
Griesinger, C., & Ernst, R. R. (1987) *J. Magn. Reson. 75*, 261−271.
Hillcoat, B. L., Nixon, P. F., & Blakley, R. L. (1967) *Anal. Biochem. 21*, 178−189.
Huennekens, F. M. (1994) *Adv. Enzyme Regul. 34*, 397−419.
Hyde, E. I., Birdsall, B., Roberts, G. C. K., Feeney, J., & Burgen, A. S. V. (1980) *Biochemistry 19*, 3738−3746.
Jackson, R. C., Hart, L. I., & Harrap, K. R. (1976) *Cancer Res. 36*, 1991−1997.
Jeener, J., Meier, B. H., Bachmann, P., & Ernst, R. R. (1979) *J. Chem. Phys. 71*, 4546−4553.
Jolivet, J., & Chabner, B. A. (1983) *J. Clin. Invest. 72*, 773−778.
Kaufman, B. T. (1974) *Methods Enzymol. 34*, 272−281.
Kay, L. E., Marion, D., & Bax, A. (1989) *J. Magn. Reson. 84*, 72−84.
Kay, L. E., Xu, G.-Y., Singer, A. U., Muhandiram, D. R., & Forman-Kay, J. D. (1993) *J. Magn. Reson. B 101*, 333−337.
Kessler, H., Griesinger, C., Kerssebaum, R., Wagner, K., & Ernst, R. R. (1987) *J. Am. Chem. Soc. 109*, 607−609.
Kraulis, P. J. (1991) *J. Appl. Crystallogr. 24*, 946−950.
Kraut, J., & Matthews, D. A. (1987) in *Biological Macromolecules and Assemblies* (Jurnak, F. A., & McPherson, A., Eds.) Vol. 3, pp 1−72, J. Wiley, New York.
Marion, D., Kay, L. E., Sparks, S. W., Torchia, D. A., & Bax, A. (1989a) *J. Am. Chem. Soc. 111*, 1515−1517.
Marion, D., Ikura, M., Tschudin, R., & Bax, A. (1989b) *J. Magn. Reson. 85*, 393−399.
Martorell, G., Gradwell, M. J., Birdsall, B., Bauer, C. J., Frenkiel, T. A., Cheung, H. T. A., Polshakov, V. I., Kuyper, L., & Feeney, J. (1994) *Biochemistry 33*, 12416−12426.
McGuire, J. J., Russell, C. A., Bolanowska, W. E., Freitag, C. M., Jones, C. S., & Kalman, T. I. (1990) *Cancer Res. 50*, 1726−1731.
McTigue, M. A., Davies, J. F., II, Kaufman, B. T., & Kraut, J. (1992) *Biochemistry 31*, 7264−7273.
Meiering, E. M., & Wagner, G. (1995) *J. Mol. Biol. 247*, 294−308.
Morgan, W. D., Birdsall, B., Polshakov, V. I., Šali, D., Kompis, I., & Feeney, J. (1995) *Biochemistry 34*, 11690−11702.
Oefner, C., D'Arcy, A., & Winkler, F. K. (1988) *Eur. J. Biochem. 174*, 377−385.
Olejniczak, E. T., & Eaton, H. L. (1990) *J. Magn. Reson. 87*, 628−632.
Piantini, U., Sørensen, O. W., & Ernst, R. R. (1982) *J. Am. Chem. Soc. 104*, 6800−6801.
Prendergast, N. J., Delcamp, T. J., Smith, P. L., & Freisheim, J. H. (1988) *Biochemistry 27*, 3664−3671.
Reyes, V. M., Sawaya, M. R., Brown, K. A., & Kraut, J. (1995) *Biochemistry 34*, 2710−2723.
Rhee, M. S., Galivan , J., Wright, J. E., & Rosowsky, A. (1994) *Mol. Pharmacol. 45*, 783−791.
Rosowsky, A., Bader, H., Cucchi, C. A., Moran, R. G., Kohler, W., & Freisheim, J. H. (1988) *J. Med. Chem. 31*, 1332−1337.
Rosowsky, A., Bader, H., & Forsch, R. A. (1989) *Pteridines 1*, 91−98.
Rosowsky, A., Bader, H., & Frei, E., III (1991) *Proc. Am. Assoc. Cancer Res. 32*, 325.
Rosowsky, A., Bader, H., Wright, J. E., Keyomarsi, K., & Matherly, L. H. (1994) *J. Med. Chem. 37*, 2167−2174.
Shaka, A. J., Lee, C. J., & Pines, A. (1988) *J. Magn. Reson. 77*, 274−293.
Sirotnak, F. M., Chello, P. L., Moccio, D. M., Piper, J. R., Montgomery, J. A., & Parham, J. C. (1980) *Biochem. Pharmacol. 29*, 3293−3298.
Sirotnak, F. M., Chello, P. L., DeGraw, J. I., Piper, J. R., & Montgomery, J. A. (1981) in *Molecular Actions and Targets for Cancer Chemotherapeutic Agents* (Sartorelli, A. C., Lazo, J. S., & Bertino, J. R., Eds.) pp 349−383, Academic Press, New York.
Soteriou, A., Carr, M. D., Frenkiel, T. A., McCormick, J. E., Bauer, C. J., Šali, D., Birdsall, B., & Feeney, J. (1993) *J. Biomol. NMR 3*, 535−546.
Stockman, B. J., Nirmala, N. R., Wagner, G., Delcamp, T. J., DeYarman, M. T., & Freisheim, J. H. (1991) *FEBS Lett. 283*, 267−269.
Stockman, B. J., Nirmala, N. R., Wagner, G., Delcamp, T. J., DeYarman, M. T., & Freisheim, J. H. (1992) *Biochemistry 31*, 218−229.
Straus, O. H., & Goldstein, A. (1943) *J. Gen. Physiol. 26*, 559−585.
Thompson, P. D., & Freisheim, J. H. (1991) *Biochemistry 30*, 8124−8130.
Vehar, G. A., & Freisheim, J. H. (1976) *Biochem. Biophys. Res. Commun. 68*, 937−941.
Vuister, G. W., & Bax, A. (1993) *J. Am. Chem. Soc. 115*, 7772−7777.
Westerhof, G. R., Schornagel, J. H., Kathmann, I., Jackman, A. L., Rosowsky, A., Forsch, R. A., Hynes, J. B., Boyle, F. T., Peters, G. J., Pinedo, H. M., & Jansen, G. (1995) *Mol. Pharmacol. 48*, 459−471.

BI963039I